

Carbon-Nanotube/ β -Ga₂O₃ Heterojunction PIN Diodes

Hunter D. Ellis, Botong Li, Haoyu Xie, Jichao Fan, Imteaz Rahaman, Weilu Gao, and Kai Fu^{a)}

Department of Electrical and Computer Engineering, The University of Utah, Salt Lake City, UT 84112, USA

β -Ga₂O₃ is gaining attention as a promising semiconductor for next-generation high-power, high-efficiency, and high-temperature electronic devices, thanks to its exceptional material properties. However, challenges such as the lack of viable p-type doping have hindered its full potential, particularly in the development of ambipolar devices. This work introduces a novel heterojunction diode (HD) that combines p-type carbon nanotubes (CNTs) with i/n-type β -Ga₂O₃ to overcome these limitations. For the first time, a CNT/ β -Ga₂O₃ hetero-p-n-junction diode is fabricated. Compared to a traditional Schottky barrier diode (SBD) with the same β -Ga₂O₃ epilayer, the CNT/ β -Ga₂O₃ HD demonstrates significant improvements, including a higher rectifying ratio (1.2×10^{11}), a larger turn-on voltage (1.96 V), a drastically reduced leakage current at temperatures up to 300 °C, and a 26.7% increase in breakdown voltage. Notably, the CNT/ β -Ga₂O₃ HD exhibits a low ideality factor of 1.02, signifying an ideal interface between the materials. These results underline the potential of CNT/ β -Ga₂O₃ heterojunctions for electronic applications, offering a promising solution to current limitations in β -Ga₂O₃-based devices.

^{a)} Author to whom correspondence should be addressed: kai.fu@utah.edu

β -Ga₂O₃ has gained significant attention as an emerging semiconductor material for next-generation high-power and high-efficiency electronic devices due to its remarkable material properties. With an ultra-wide bandgap of 4.9 eV, a high critical breakdown electric field of 8 MV/cm, and an exceptional Baliga's figure of merit of 136 GW/cm⁻², β -Ga₂O₃ is particularly promising for high-power switching applications¹⁻⁴, enabling high breakdown voltages, low on-resistance, and low power losses⁵. These properties also enhance its resilience, enabling exceptional performance in high-temperature and radiation-rich environments^{5, 6}. Recent advancements in growth techniques have significantly reduced production costs of β -Ga₂O₃ substrates, further its suitability in these applications⁷⁻⁹.

Despite these advantages, the lack of viable p-type doping in β -Ga₂O₃ presents a significant challenge, as it hinders the development of ambipolar devices and limits the material's design versatility¹⁰. On the other hand, β -Ga₂O₃ based Schottky barrier diodes (SBD) have shown severely increased leakage current and reduced breakdown voltage at elevated temperatures due to the relatively low barrier height^{5, 11, 12}. To address these limitations, heterojunction diodes (HDs) have been widely adopted by integrating a p-type material with n-type β -Ga₂O₃. Various p-type materials, including NiO, Cr₂O₃, and diamond, have been explored for forming the heterojunctions¹³⁻¹⁹. Some challenges of these materials have also been reported, such as hole concentration thermal stability of NiO²⁰, and low breakdown voltages of Cr₂O₃¹⁵. Researchers have been actively exploring more p-type materials for the HDs.

Two-dimensional materials offer another promising avenue due to their self-passivating properties²¹. Materials such as graphene, black phosphorus, and p-WSe₂ have been investigated, while graphene enables an exceptionally high critical electric field of 5.2 MV/cm²²⁻²⁴. Carbon nanotubes (CNTs) have also emerged as strong candidates for heterojunction applications, such as

solar cells and photocatalysts, due to their outstanding properties, including high field-effect mobility, tunable bandgaps, and the capacity to sustain high current densities²⁵⁻³³, making CNTs another potential p-type material for Ga₂O₃ heterojunctions.

In this work, we have studied the performance of a hetero-p-n-junction based on p-type CNT and i/n-type Ga₂O₃ for the first time. Key parameters, including ideality factor, barrier height, leakage current, and breakdown voltage, are systematically analyzed. Compared with Schottky diodes on the same epilayer, the CNT/ β -Ga₂O₃ HD shows a larger turn-on voltage, larger rectifying ratio, reduced reverse leakage current up to 300 °C, and increased breakdown voltage. The CNT/Ga₂O₃ diode also shows a low ideality factor of 1.02 compared to other HD diodes reported.

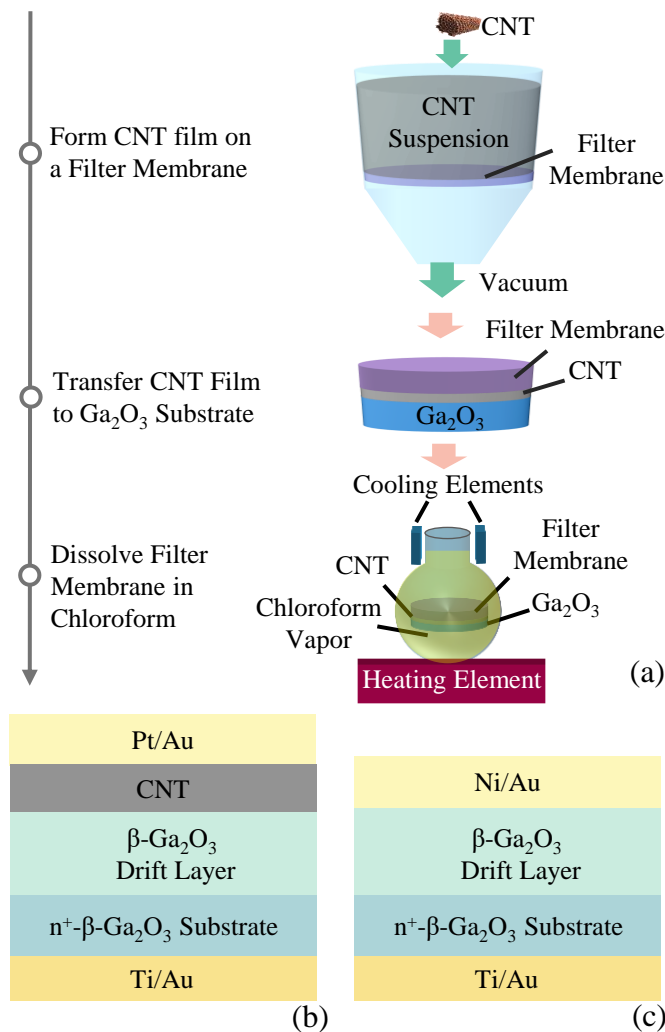


FIG. 1. (a) Schematics of the CNT deposition process flow. Structures of (b) the CNT/ β -Ga₂O₃ HD and (c) the β -Ga₂O₃ SBD on the same epilayer.

The CNT thin film deposition was accomplished by first preparing a wafer-scale (2-inch diameter) randomly oriented CNT film using a vacuum filtration method³⁴. Specifically, CNT powder was dispersed in a sodium deoxycholate (DOC) surfactant solution and subjected to tip sonication and ultracentrifugation to break down CNT bundles and remove impurities and undispersed bundles. The CNT suspension was then diluted while maintaining a DOC concentration higher than its critical micelle concentration. A fast vacuum filtration was performed to produce the film, which was left on the filtration system to dry completely. The dried film on the filter membrane was transferred onto the β -Ga₂O₃ using a wet transfer process³⁵. A droplet of water was applied to the target substrate, and the CNT film was inverted, placing the CNT side in contact with the wet substrate while leaving the polycarbonate membrane above. Once the water evaporated, the sample was exposed to chloroform vapor inside a reflux condenser to dissolve and remove the polycarbonate membrane. The residual chloroform was removed by repeating the process with isopropyl alcohol, yielding a clean, randomly oriented CNT film. This CNT thin film deposition process is outlined in Fig. 1(a).

The β -Ga₂O₃ wafer was sourced from Novel Crystal Technology, Inc., and featured a 10 μ m-thick drift layer with a doping concentration of 1×10^{16} cm⁻³. The β -Ga₂O₃ epilayer was grown on a (001) Sn doped n⁺- β -Ga₂O₃ substrate. A Pt (50 nm)/Au (80 nm) alloy was sputtered to form ohmic contacts on the CNT film, and lift-off was used to remove the excess alloy. Pt was used instead of Ni for the CNT contact because Pt has less contact resistance with CNT. O₂ plasma was used to do a self-aligned mesa etch of the CNT. A back contact was formed by depositing Ti (50 nm)/Au (250 nm) on the Ga₂O₃ substrate surface. The CNT/ β -Ga₂O₃ structure is shown in Fig. 1(b).

A Ga₂O₃ SBD was also fabricated as a reference for the CNT/ β -Ga₂O₃ HD, and the structure is shown in Fig. 1(c). The same β -Ga₂O₃ wafer was used for the SBD fabrication as the HD. Ni(50 nm)/Au(100 nm) Schottky contacts were formed on the top surface, and lift-off was employed using the same photoresists as the HD to form the individual devices. The back contact was formed by depositing Ti (50 nm)/Au (250 nm). The forward I - V , along with the C - V measurements, were characterized using a 4200A-SCS parameter analyzer. The breakdown voltage was measured with a Keithley 2470 Source Meter.

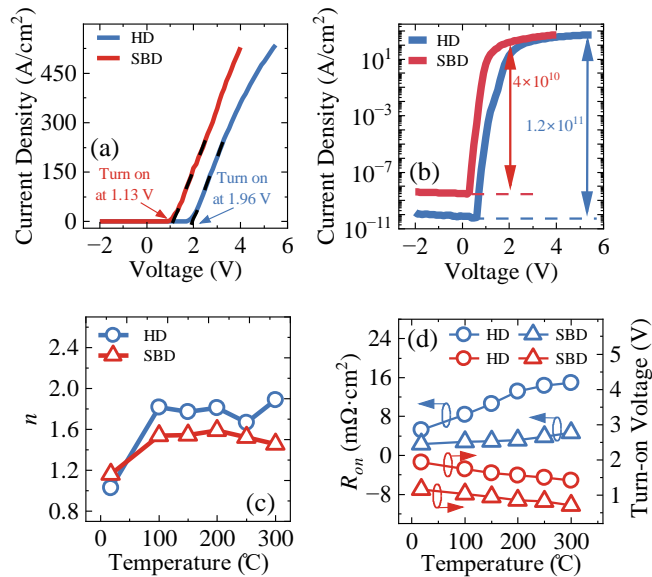


FIG. 2. Comparison of forward performance of the CNT/ β -Ga₂O₃ HD and β -Ga₂O₃ SBD. (a) I - V curves in linear scale. (b) I - V curves in semi-log scale. (c) Ideality factor at various temperatures. (d) Differential on-resistance (R_{on}), and the turn-on voltages at different temperatures up to 300 °C.

Figures 2(a) and (b) compare the forward I - V characteristics of the CNT/ β -Ga₂O₃ HD and the SBD in both linear (Fig. 2(a)) and logarithmic (Fig. 2(b)) scales. The HD exhibits a higher turn-on voltage of 1.96 V compared to the SBD with a turn-on voltage of 1.13 V. This increase in turn-on voltage is indicative of an increased barrier height. Furthermore, the HD can achieve the same current density level as the SBD of 535 A/cm² at 5 V, demonstrating efficient carrier transportation

across the heterojunction. The HD also shows significantly reduced reverse leakage current compared to the SBD, as evidenced in Fig. 2(b), further supporting the hypothesis of an increased barrier height or MIS structure formation. The similar on-current and reduced leakage current result in a high rectifying ratio of 1.2×10^{11} for the HD, which is three times larger than the SBD, which has a rectifying ratio of 4×10^{10} .

Figure 2(c) presents the temperature dependence of the ideality factor (n) for both devices from 18 °C (room temperature) to 300 °C. At 18 °C, the HD exhibits a low ideality factor of 1.02, compared to the SBD with an ideality factor of 1.16. The ideality factor of nearly 1 for the HD demonstrates an ideal nature of the interface between the CNT and the β -Ga₂O₃. The ideality factor of the HD increases with temperature, consistent with the behavior observed in other β -Ga₂O₃ HDs, often attributed to effects such as interface states or tunneling¹⁴. Similarly, the SBD's ideality factor increases with temperature, potentially due to barrier inhomogeneities or interface states³⁶.

Figure 2(d) presents the differential on-resistance (R_{on}) and the turn-on voltage from 18 °C to 300 °C. The SBD exhibited a lower R_{on} than that of the HD at all temperatures, a trend previously reported for NiO/ β -Ga₂O₃ HDs^{5,37,38}. Both devices show an increase in R_{on} with temperature, due to the reduced carrier mobility in Ga₂O₃ due to phonon scattering³⁹. The turn-on voltage decreases with temperature for both the HD and the SBD at a rate of 1.6 mV/K, which is due to the increased reverse saturation current density and reduced built-in potential resulting from the increased intrinsic carrier concentration at elevated temperatures. The dependence of the voltage on the reverse saturation current density is given in Eq. (1),

$$V = \frac{k_b T}{q} \times \exp\left(\frac{J}{J_0} + 1\right) \quad (1)$$

where V is the applied voltage, k_b is the Boltzmann constant, T is the temperature, J is the current density, and J_0 is the reverse saturation current⁴⁰.

The decrease in the bandgap of Ga₂O₃ with temperature could have also contributed to the decreased turn-on voltage^{41, 42}.

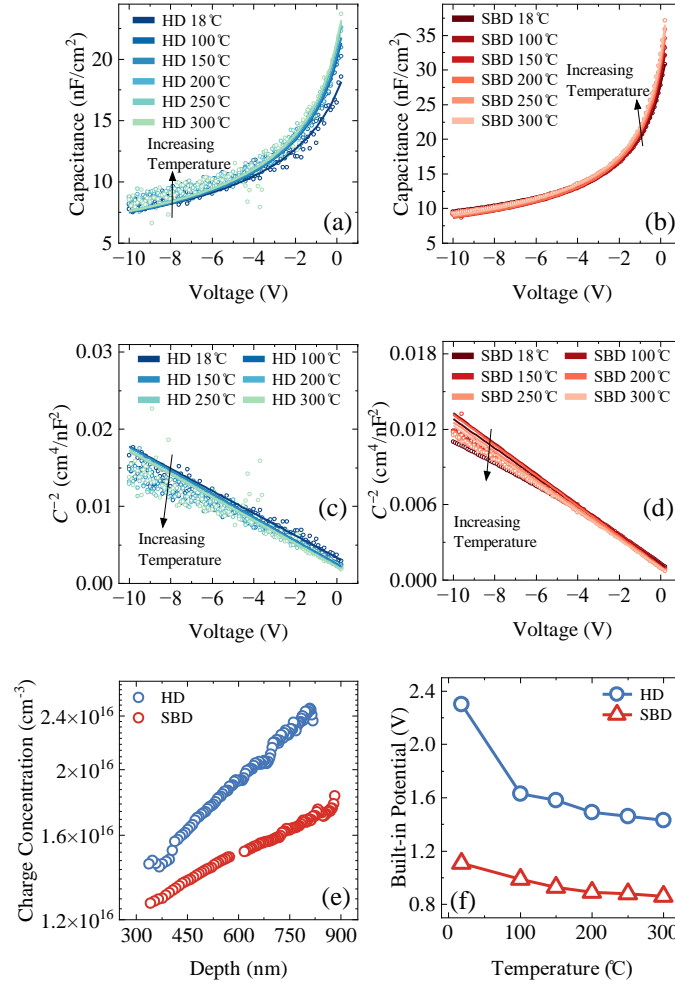


FIG. 3. C - V curves of (a) CNT/ β -Ga₂O₃ HD and (b) the β -Ga₂O₃ SBD at different temperature. C^{-2} - V plots for (c) CNT/ β -Ga₂O₃ HD and (d) the β -Ga₂O₃ SBD at different temperatures. (e) Derived doping concentration in the epilayers. (f) Derived built-in barrier height of the CNT/ β -Ga₂O₃ HD and the β -Ga₂O₃ SBD at different temperatures.

Figure 3(a) and (b) display the C - V curves for the HD (Fig. 3(a)) and the SBD (Fig. 3(b)) from 18 °C to 300 °C. the HD shows smaller capacitance than the SBD due to the enhanced depletion depth in the HD at the same biases. Figure 3(c) and (d) present the C^{-2} - V characteristics of the HD

(Fig. 3(c)) and SBD (Fig. 3(d)) from 18 °C to 300 °C. The C^{-2} - V curves reveal variations in the built-in potential (V_{bi}), with the HD exhibiting a V_{bi} of 2.3 V and the SBD showing a V_{bi} of 1.2 V at 18 °C, providing evidence of the increased barrier height in the HD. Figure 3(e) shows the doping concentration in the Ga₂O₃ epilayers at room temperature as a function of depth, derived from the C - V data. The doping concentration was only determined for the low-doped β -Ga₂O₃ side due to the CNT's high intrinsic p-type doping concentration^{43, 44}. While some differences are observed between the HD and SBD, they fall within the $\pm 50\%$ variation in doping concentration expected from the wafer manufacturer. The derived built-in potentials at different temperatures are presented in Fig. 3(f). The built-in potentials of both the HD and the SBD decrease with increasing temperature, which will cause the increase of leakage current at reverse biases⁴⁵.

Figure 4(a) compares the breakdown voltages of the HD and SBD. Without edge termination, the HD achieves a breakdown voltage of 912 V, significantly higher than the 723 V observed for the SBD. Additionally, the HD exhibits a significantly low leakage current, as illustrated in Fig. 4(a). The reverse I - V curves from 0–200 V across the temperature range of 18 °C to 300 °C are presented in Fig. 4(b), and they highlight the HD's exceptional thermal stability, with leakage current at 300 °C smaller than the SBD at 18 °C. These results demonstrate the enhanced breakdown voltage, reduced leakage current, and improved thermal robustness of the CNT/ β -Ga₂O₃ HD compared to the SBD.

The leakage mechanism of the SBD was explored, and it was found to be a combination of Poole Frenkel emission (PFE) and variable range hopping (VRH). The measured data compared to the simulated PFE and VRH current is shown in Fig. 4(c). The PFE leakage current was modeled using Eq. (2),

$$J_{PFE} = J_0 \exp\left(\frac{\beta E^{0.5}}{k_b T}\right) \quad (2)$$

where J_{PFE} is the leakage current due to PFE, β is the lowering of the barrier, and E is the electric field at the interface⁴⁶.

The VRH leakage current was modeled using Eq. (3),

$$J_{VRH} = J_0 \exp \left(C \frac{qE}{2k_b T} \left(\frac{T}{T_0} \right)^{1/4} \right) \quad (3)$$

where J_{VRH} is the leakage due to VRH, C is a constant, q is the charge of an electron, and T_0 is the characteristic temperature⁴⁷.

The leakage mechanism of the HD was investigated by analyzing the dependence of the electric field on the leakage current based on the mechanisms listed in Table I. Figure 4(d) shows that the leakage current follows a relationship of $\log(I)/\log(E) \geq 2$, where I is the leakage current and E is the electric field. Based on Table I, the primary leakage mechanism of the HD is the space charge limited current (SCLC)⁴⁸. Other possible mechanisms including PFE⁴⁶, and surface leakage⁴⁶, can also contribute to the leakage current. A comparison of key electrical parameters of the HD in this work and other reported Ga₂O₃ HDs are shown in Table II. The HD diode in this work achieves a very high rectifying ratio, the lowest ideality factor, a moderate R_{on} , and a decent turn-on voltage compared to the reported HDs with other p-type materials.

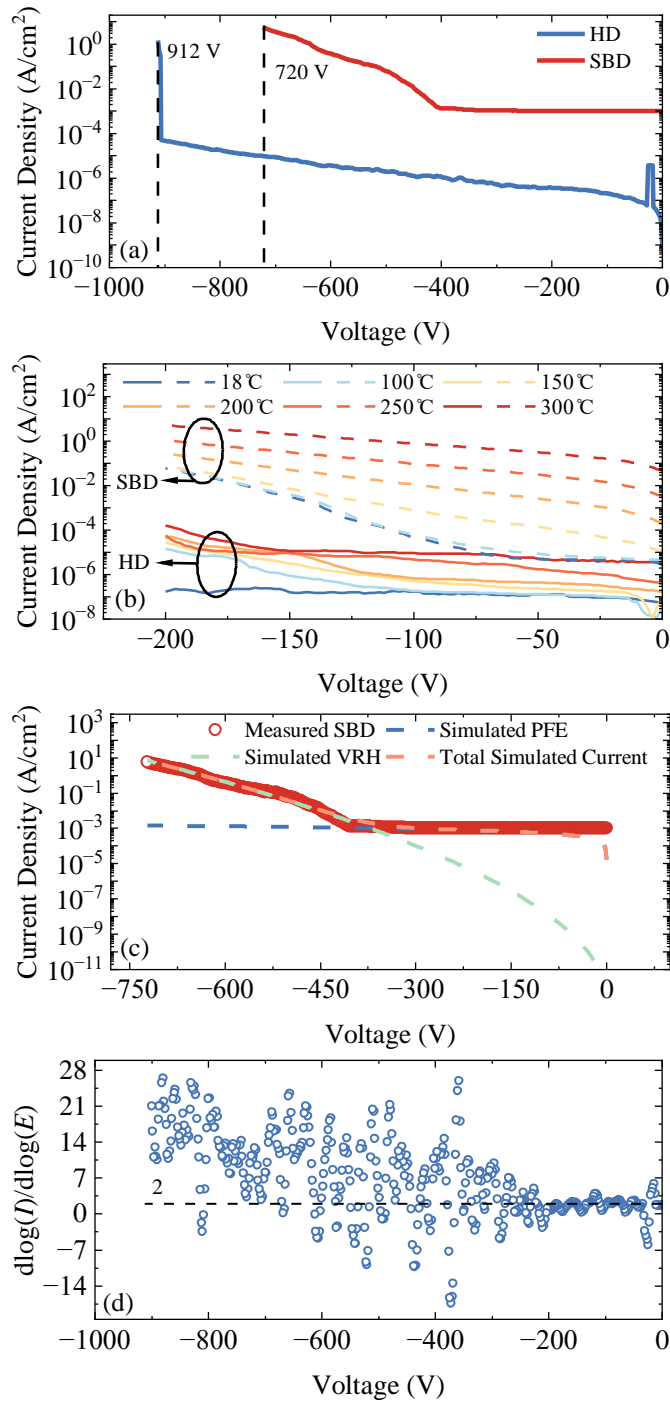


FIG. 4. (a) Reverse I - V curves and breakdown voltages of the CNT/ β -Ga₂O₃ HD and the β -Ga₂O₃ SBD at room temperature. (b) Reverse I - V curves at high temperatures up to 300 °C. (c) Comparison of the measured SBD leakage current, simulated leakage current due to PFE, and

VRH mechanisms. (d) $\text{dlog}(I)/\text{dlog}(E)$ vs voltage derived from the reverse I - V curve of the CNT/ β - Ga_2O_3 HD.

Most research on CNTs focuses on their in-plane properties, while the vertical (out-of-plane) transport characteristics explored in this work have been rarely investigated. Another potential role of the CNT here contributing to the reduced leakage current could be the CNTs acting as an insulating dielectric. In this scenario, the forward current would rely on the carrier tunneling through the CNTs. Given the CNT layer's thickness (30 nm) and a calculated relative permittivity of approximately two (as shown in Fig. 5(a)), derived from C - V measurements taken on the device shown in the inset of Fig. 5(a) across frequencies from 1 MHz to 10 kHz, tunneling would produce negligible forward current while the forward current density achieved by the HD is almost the same as the SBD. So, we can confirm the p-type role of the CNT here. Furthermore, the experimental findings align well with the band diagram of a heterojunction p-n diode, as illustrated in Fig. 5(b). The configuration explains the increased barrier height, higher turn-on voltage, reduced leakage current, and comparable current density to the SBD.

Table I. Common leakage mechanisms in diodes.

Mechanism	Equation	Differential Slope	Reference
SCLC	$I = \frac{9\epsilon\mu E^n}{8W^3} (n \leq 2)$	$\frac{\text{dlog}(I)}{\text{dlog}(E)} \propto n$	48
Poole-Frankel	$I = I_0 \exp\left(\frac{\beta E^{0.5}}{k_b T}\right)$	$\frac{\text{dlog}(\ln(I))}{\text{dlog}(E)} \propto 0.5$	46
Surface Leakage	$I \propto \frac{E}{q}$	$\frac{\text{dlog}(I)}{\text{dlog}(E)} = 1$	46

ϵ : permittivity, W : depletion width, and μ : mobility.

Table II. Comparison of reported Ga_2O_3 HDs with different p-type materials.

p-Material on Ga_2O_3	Rectifying Ratio	Turn-on Voltage (V)	BV (V)	R_{on} ($\text{m}\Omega/\text{cm}^2$)	Ideality Factor	Reference
CNT	1.2×10^{11}	1.96	912	5.2	1.02	This Work

NiO	N.A.	2.4	1059	3.5	1.22	16
NiO	10^{10}	2.2	1860	10.6	1.8	49
NiO	10^8	1.65	1630	4.1	1.27	14
Cr ₂ O ₃	10^4	1.08	390	5.34	1.08	15
NiO	2.9×10^{12}	2.2	8000	7.8	...	50
CuO _x	10^8	...	2780	6.46	1.7	51

In conclusion, CNT/ β -Ga₂O₃ HDs have been fabricated, demonstrating superior performance compared to a reference β -Ga₂O₃ Schottky barrier diode (SBD). The CNT/ β -Ga₂O₃ HDs achieve a rectifying ratio three times higher, a 26.7% increase in breakdown voltage, a reduction in reverse leakage current by over two orders of magnitude, and an ideality factor close to 1. The advantage persists at elevated temperatures, with the HD consistently demonstrating significantly

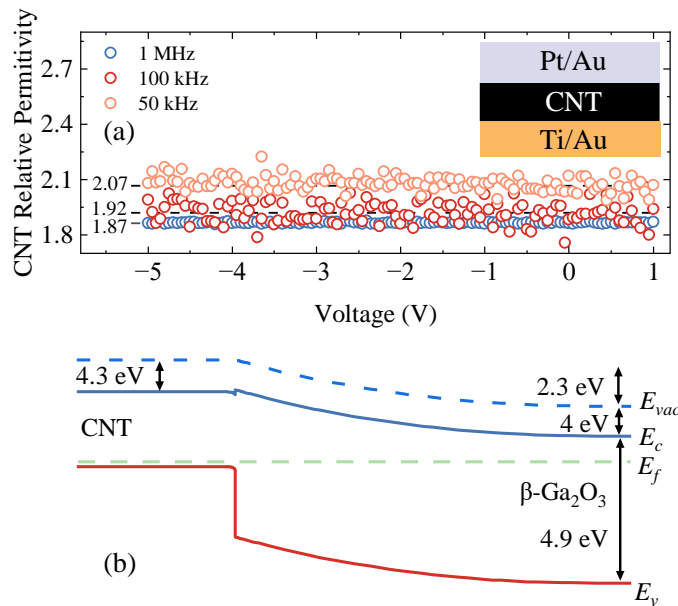


FIG. 5. (a) Relative permittivity of CNT from 10 kHz to 1 MHz, the inset shows the capacitor structure that was used to measure the C-V. (b) Band diagram for the CNT/ β -Ga₂O₃ HD.

lower leakage current up to 300 °C The HD also matched the SBD in forward current density, reaching 535 A/cm², confirming efficient carrier transportation across the heterojunction. These

findings establish CNT as a promising p-type material for β -Ga₂O₃ heterojunction diodes, offering significant potential for high-power and high-temperature applications.

AUTHOR DECLARATIONS

Conflict of Interest

The authors have no conflicts to disclose.

Author Contributions

Hunter Ellis: Fabrication (lead); Data curation (lead); Formal analysis (lead); Investigation (lead); Methodology (lead); Writing original draft (lead). Botong Li: Fabrication (equal); Data curation (equal). Jichao Fan: Writing original draft (supporting); Fabrication (equal). Haoyu Xie: Writing original draft (supporting); Fabrication (supporting). Imteaz Rahaman: Writing – review & editing (supporting). Weilu Gao: Conceptualization (equal), Resources (equal), Writing – review & editing (equal). Kai Fu: Conceptualization (lead); Supervision (lead); Project administration (lead); Resources (lead).

DATA AVAILABILITY

The data that support the findings of this study are available from the corresponding authors upon reasonable request.

Acknowledgment

The device fabrication was performed at the Nanofab at the University of Utah. This work is supported in part by the University of Utah start-up fund and PIVOT Energy Accelerator Grant U-7352FuEnergyAccelerator2023. X. H., J. F., and W. G. acknowledge the support from National Science Foundation through grants no. 2230727 and 2321366.

REFERENCES

- (1) Galazka, Z. β -Ga₂O₃ for wide-bandgap electronics and optoelectronics. *Semiconductor Science and Technology*, **2018**, 33, no. 11, 113001.
- (2) Pearton, S.; Yang, J.; Cary, P.; Ren, F.; Kim, J.; Tadjer, M.; Mastro, M. review of Ga₂O₃ materials, processing, and devices. *Applied Physics Reviews*, **2018**, 5, no. 1, 011301.
- (3) Rahaman, I.; Ellis, H.; Chang, C.; Mudiyansele, D.; Xu, M.; Da, B.; Fu, H.; Zhao, Y.; Fu, F. Epitaxial Growth of Ga₂O₃: A Review. *Materials*, **2024**, 17, no. 17, 4261.
- (4) Dong, P.; Zhang, J.; Yan, Q.; Liu, Z.; Ma, P.; Zhou, H.; Hao, Y. 6 kV/3.4 mΩ·cm² Vertical β -Ga₂O₃ Schottky Barrier Diode With BV²/R_{on,sp} Performance Exceeding 1-D Unipolar Limit of GaN and SiC. *IEEE Electron Device Letters*, **2022**, 43, no. 5, 765-768.
- (5) Li, J.; Chiang, C.; Xia, X.; Wan, H.; Ren, F.; Pearton, S. Superior high temperature performance of 8 kV NiO/Ga₂O₃ vertical heterojunction rectifiers. *Journal of Materials Chemistry C*, **2023**, 11, no. 23, 7750-7757.
- (6) Pearton, S.; Yang, J.; Cary IV, P.; Ren, F.; Kim, J. *Gallium Oxide* (Gallium Oxide). Elsevier, **2019**.
- (7) Higashiwaki, M.; Sasaki, K.; Murakami, H.; Kumagai, Y.; Koukitu, A.; Kuramata, A.; Masui, T.; Yamakoshi, S. Recent progress in Ga₂O₃ power devices. *Semiconductor Science and Technology*, **2016**, 31, no. 3, 034001.
- (8) Baldini, M.; Galazka, Z.; Wagner, G. Recent progress in the growth of β -Ga₂O₃ for power electronics applications. *Materials Science in Semiconductor Processing*, **2018**, 78, 132-146.
- (9) Yuan, Y.; Hao, W.; Mu, W.; Wang, Z.; Chen, X.; Liu, Q.; Xu, G.; Wang, C.; Zhou, H.; Zou, Y. Toward emerging gallium oxide semiconductors: A roadmap. *Fundamental Research*, **2021**, 1, no. 6, 697-716.
- (10) Green, A.; Speck, J.; Xing, G.; Moens, P.; Allerstam, F.; Gumaelius, K.; Neyer, T.; Arias-Purdue, A. Mehrotra, V.; Kuramata, A. β -Gallium oxide power electronics. *Apl Materials*, **2022**, 10, no. 2, 029201.
- (11) Ellis, H.; Jia, W.; Rahaman, I.; Hillas, A.; Li, B.; Scarpulla, M.; Sensale Rodriguez, B.; Fu, K. Degradation of 2.4-kV Ga₂O₃ Schottky Barrier Diode at High Temperatures up to 500 C. *arXiv preprint arXiv:2503.14805*, **2025**.
- (12) Sun, R.; Balog, A.; Yang, H.; Alem, N.; Scarpulla, M. Degradation of β -Ga₂O₃ vertical Ni/Au Schottky diodes under forward bias. *IEEE Electron Device Letters*, **2023**.
- (13) Egbo, K.; Garrity, E.; Callahan, W.; Chae, C.; Lee, C.; Tellekamp, B.; Hwang, J.; Stevanovic, V.; Zakutayev, A. NiGa₂O₄ interfacial layers in NiO/Ga₂O₃ heterojunction diodes at high temperature. *Applied Physics Letters*, **2024**, 124, no. 17, 173512.
- (14) Hao, W.; He, Q.; Zhou, K.; Xu, G.; Xiong, W.; Zhou, X.; Jian, G.; Chen, C.; Zhao, X.; Long, S. Low defect density and small I–V curve hysteresis in NiO/ β -Ga₂O₃ pn diode with a high PFOM of 0.65 GW/cm². *Applied Physics Letters*, **2021**, 118, no. 4, 043501.
- (15) Callahan, W.; Egbo, K.; Lee, C.; Ginley, D.; O'Hayre, R.; Zakutayev, A. Reliable operation of Cr₂O₃: Mg/ β -Ga₂O₃ p–n heterojunction diodes at 600° C. *Applied Physics Letters*, **2024**, 124, no. 15, 15354.
- (16) Lu, X.; Zhou, X.; Jiang, H.; Wei Ng, K.; Chen, Z.; Pei, Y.; Lau, K.; Wang, G. 1-kV Sputtered p-NiO/n-Ga₂O₃ Heterojunction Diodes With an Ultra-Low Leakage Current Below 1 μ A/cm². *IEEE Electron Device Letters*, **2020**, 41, no. 3, 449-452.
- (17) Gong, H.; Chen, X.; Xu, Y.; Ren, F.; Gu, S.; Ye, J. A 1.86-kV double-layered NiO/ β -Ga₂O₃ vertical p–n heterojunction diode. *Applied Physics Letters*, **2020**, 117, no. 2, 022104.

- (18) Wang, C.; Gong, H.; Lei, W.; Cai, Y.; Hu, Z.; Xu, S.; Liu, Z.; Feng, Q.; Zhou, H.; Ye, J. Demonstration of the p-NiO_x/n-Ga₂O₃ heterojunction gate FETs and diodes with BV²/R_{on,sp} figures of merit of 0.39 GW/cm² and 1.38 GW/cm². *IEEE Electron Device Letters*, **2021**, 42, no. 4, 485-488.
- (19) Rahaman, I.; Sultana, M.; Medina, R.; Emu, I.; Haque, A. Optimization of electrostatic seeding technique for wafer-scale diamond fabrication on β-Ga₂O₃. *Materials Science in Semiconductor Processing*, **2024**, 184, 108808.
- (20) Lu, X.; Deng, Y.; Pei, Y.; Chen, Z.; Wang, G. Recent advances in NiO/Ga₂O₃ heterojunctions for power electronics. *Journal of Semiconductors*, **2023**, 44, no. 6, 061802.
- (21) Lemme, M.; Akinwande, D.; Huyghebaert, C.; Stampfer, C.; 2D materials for future heterogeneous electronics. *Nature communications*, **2022**, 13, no. 1, 1392.
- (22) Leblanc, C.; Mudiyansele, D.; Song, D.; Zhang, H.; Davydov, A.; Fu, H.; Jariwala, D. Vertical van der Waals heterojunction diodes comprising 2D semiconductors on 3D β-Ga₂O₃. *Nanoscale*, **2023**, 15, no. 23, 9964-9972.
- (23) Yan, X.; Esqueda, I.; Ma, J.; Tice, J.; Wang, H. High breakdown electric field in β-Ga₂O₃/graphene vertical barristor heterostructure. *Applied Physics Letters*, **2018**, 112, no. 3.
- (24) Kim, J.; Mastro, M.; Tadjer, M.; Kim, J. Heterostructure WSe₂-Ga₂O₃ junction field-effect transistor for low-dimensional high-power electronics. *ACS applied materials & interfaces*, **2018**, 10, no. 35, 29724-29729.
- (25) Li, X.; Lv, Z.; Zhu, H. Carbon/silicon heterojunction solar cells: state of the art and prospects. *Advanced Materials*, **2015**, 27, no. 42, 6549-6574.
- (26) Jung, Y.; Li, X.; Rajan, N.; Taylor, A.; Reed, M. Record high efficiency single-walled carbon nanotube/silicon p-n junction solar cells. *Nano Letters*, **2013**, 13, no. 1, 95-99.
- (27) Di, J.; Yong, Z.; Zheng, X.; Sun, B.; Li, Q. Aligned carbon nanotubes for high-efficiency Schottky solar cells. *Small*, **2013**, 9, no. 8, 1367-1372.
- (28) Zhao, X.; Wu, H.; Yang, L.; Wu, Y.; Sun, Y.; Shang, Y.; Cao, A. High efficiency CNT-Si heterojunction solar cells by dry gas doping. *carbon*, **2019**, 147, 164-171.
- (29) Scagliotti, M.; Salvato, M.; Frezza, F.; Catone, D.; Mario, L.; Boscardin, M.; Crescenzi, M.; Castrucci, P. Carbon nanotube film/silicon heterojunction photodetector for new cutting-edge technological devices. *Applied Sciences*, **2021**, 11, no. 2, 606.
- (30) Yu, H.; Quan, X.; Chen, S.; Zhao, H.; Zhang, Y. TiO₂-carbon nanotube heterojunction arrays with a controllable thickness of TiO₂ layer and their first application in photocatalysis. *Journal of Photochemistry and Photobiology A: Chemistry*, **2008**, 200, no. 2-3, 301-306.
- (31) Mo, Y.; Guo, C.; Wang, W.; Liu, P.; Guo, J.; Chen, J.; Deng, X.; Li, G. Interface passivation treatment enables GaAs/CNT heterojunction solar cells over 19% efficiency. *Nano Energy*, **2024**, 131, 110247.
- (32) Biswas, C.; Lee, S.; Ly, T.; Ghosh, A.; Dang, Q.; Lee, Y. Chemically doped random network carbon nanotube p-n junction diode for rectifier. *ACS nano*, **2011**, 5, no. 12, 9817-9823.
- (33) Hu, L.; Hecht, D.; Gruner, G. Carbon nanotube thin films: fabrication, properties, and applications. *Chemical reviews*, **2010**, 110, no. 10, 5790-5844.
- (34) Wu, Z.; Chen, Z.; Du, X.; Logan, J.; Sippel, J.; Nikolou, M.; Kamaras, K.; Reynolds, J.; Tanner, D.; Hebard, A. Transparent, conductive carbon nanotube films. *Science*, **2004**, 305, no. 5688, 1273-1276.

- (35) He, X.; Gao, W.; Xie, L.; Li, B.; Zhang, Q.; Lei, S.; Robinson, J.; Hároz, E.; Doorn, S.; Wang, W. Wafer-scale monodomain films of spontaneously aligned single-walled carbon nanotubes. *Nature nanotechnology*, **2016**, 11, no. 7, 633-638.
- (36) Ahaitouf, A.; Srour, H.; Hamady, S.; Fressengeas, N.; Ougazzaden, A.; Salvestrini, J. Interface state effects in GaN Schottky diodes. *Thin Solid Films*, **2012**, 522, 345-351.
- (37) Sharma, S.; Zeng, K.; Saha, S.; Singiseti, U. Field-plated lateral Ga₂O₃ MOSFETs with polymer passivation and 8.03 kV breakdown voltage. *IEEE Electron Device Letters*, **2020**, 41, no. 6, 836-839.
- (38) Dong, P.; Zhang, J.; Yan, Q.; Liu, Z.; Ma, P.; Zhou, H.; Hao, Y.; 6 kV/3.4 mΩ·cm² Vertical β-Ga₂O₃ Schottky Barrier Diode With BV 2/R_{on,sp} Performance Exceeding 1-D Unipolar Limit of GaN and SiC. *IEEE Electron Device Letters*, **2022**, 43, no. 5, 765-768.
- (39) Wang, B.; Xiao, M.; Yan, X.; Wong, H.; Ma, J.; Sasaki, K.; Wang, H.; Zhang, Y. High-voltage vertical Ga₂O₃ power rectifiers operational at high temperatures up to 600 K. *Applied Physics Letters*, **2019**, 115, no. 26, 263503.
- (40) Kwok, K.; Simon, N.; Sze, M. *Physics of semiconductor Devices*. NJ, USA: John Wiley & Sons, incorporated, 2006.
- (41) Karomi, I.; Kassim, Y.; Salih, H.; Al-Ghamdi, M. "Temperature dependence of electrical and optical characteristics of InAsP laser diode," in *Journal of Physics: Conference Series*, 2021, vol. 1963, no. 1: IOP Publishing, p. 012047.
- (42) Varshni, Y. Temperature dependence of the energy gap in semiconductors. *physica*, **1967**, 34, no. 1, 149-154.
- (43) Derycke, V.; Martel, R.; Appenzeller, J.; Avouris, P. Controlling doping and carrier injection in carbon nanotube transistors. *Applied Physics Letters*, **2002**, 80, no. 15, 2773-2775.
- (44) Kang, D.; Park, N.; Ko, J.; Bae, E.; Park, W. Oxygen-induced p-type doping of a long individual single-walled carbon nanotube. *Nanotechnology*, **2005**, 16, no. 8, 1048.
- (45) Maeda, T.; Okada, M.; Ueno, M.; Yamamoto, Y.; Kimoto, T.; Horita, M.; Suda, J. Temperature dependence of barrier height in Ni/n-GaN Schottky barrier diode. *Applied Physics Express*, **2017**, 10, no. 5, 051002.
- (46) Han, D.; Oh, C.; Kim, H.; Shim, J.; Kim, K.; Shin, D. Conduction mechanisms of leakage currents in InGaN/GaN-based light-emitting diodes. *IEEE Transactions on Electron Devices*, **2014**, 62, no. 2, 587-592.
- (47) Guo, X.; Zhong, Y.; Chen, X.; Zhou, Y.; Su, S.; Yan, S.; Liu, J.; Sun, X.; Sun, Q.; Yang, H. Reverse leakage and breakdown mechanisms of vertical GaN-on-Si Schottky barrier diodes with and without implanted termination. *Applied Physics Letters*, **2021**, 118, no. 24.
- (48) Kim, J.; Kim, J.; Tak, Y.; Kim, J.; Hong, H.; Yang, M.; Chae, S.; Park, J.; Park, Y.; Chung, U. Investigation of reverse leakage characteristics of InGaN/GaN light-emitting diodes on silicon. *IEEE electron device letters*, **2012**, 33, no. 12, 1741-1743.
- (49) Gong, H.; Chen, X.; Xu, Y.; Ren, F.; Gu, S.; Ye, J. A 1.86-kV double-layered NiO/β-Ga₂O₃ vertical p-n heterojunction diode. *Applied Physics Letters*, **2020**, 117, no. 2, 022104.
- (50) Li, J.; Wan, H.; Chiang, C.; Xia, X.; Yoo, T.; Kim, H.; Ren, F.; Pearton, S. Reproducible NiO/Ga₂O₃ vertical rectifiers with breakdown voltage > 8 kV. *Crystals*, **2023**, 13, no. 6, 886.

- (51) Wang, X.; Li, M.; He, M.; Lu, H.; Chun-Zhang, C.; Jiang, Y.; Wen, K.; Du, F.; Zhang, Y.; Deng, C. Optimization of CuO./Ga₂O₃ Heterojunction Diodes for High-Voltage Power Electronics. *Nanomaterials*, **2025**, 15, no. 2, 87.